Proceedings of the 28th IEEE
EMBS Annual International Conference
New York City, USA, Aug 30-Sept 3, 2006

Brain Tissue Mapping and Segmentation by MRI-based Blind-Source-Separation Techniques

Eldad Vizel, Ehud Orian, David Carasso, and Yehoshua Y. Zeevi

***Abstract*— Brain or any other tissue signatures are considered to be linear combinations of tissue components. Mixtures of such tissue components are "blindly" separated by means of geometrical sparse component analysis. The original set of at least two MR images, acquired by using the spin-echo or spoiled FLASH techniques with specific set of Tr and Te, are sparsified by using multiple wavelets and curvelets. The algorithms and techniques are investigated by separating simulated MRI images, where the ground truth is available. They are then applied to clinical data. Both iterative FCM and robust regression lend themselves to good estimation of the mixing matrix and thereby separation of the tissue components. Further improvements are discussed.**

I. INTRODUCTION

This study addresses the problem of brain tissue classification by means of MRI. We consider it as a Blind Source Separation (BSS) problem. The observed set of multi-contrast MR images is modeled, accordingly, as linear mixtures of tissue components, represented in the form of "source" images. Each of these sources is related to a distinct resonance characteristic (reflecting the Chemical Shift) [1]. It therefore identifies the signature of a tissue component such as water or fat. Since neither the sources, nor the mixing coefficients, are known, this type of inverse (unmixing) problem is known as a BSS problem.

BSS addresses the ill-posed problem of separating a set of given mixtures x_i into the set of sources s_i. It is assumed that each of the mixtures results from different linear combination of the sources, presented in vector form as follows:

$$X(\gamma) = A \cdot S(\gamma) + n(\gamma), \tag{1}$$

where n is additive noise. Simply put, S is in our case a vector of m unknown tissue components, A is a $n \times m$ $(n \leq m)$ linear mixing matrix, and X is the vector of n observed mixtures, the sensor data, which is the only available set of data. γ is the scalar or vector of independent variable.

Manuscript received April 24, 2006. This research has been supported by the HASSIP Research Network Program, sponsored by the European Commission and by the Ollendorff Minerva Center for Vision and Image Sciences. We would like to acknowledge Tal Hendel of the Technion Biomedical Engineering Department for assistance with MR image acquisition.

E. Vizel is with the Biomedical Engineering Department, Technion - Israel Institute of Technology, Haifa, 32000 Israel (phone: +972-54-4485847; fax: +972-4-8293315; e-mail: eldadv@tx.technion.ac.il).

E. Orian, D. Carasso, and Y.Y. Zeevi are with the Electrical Engineering Department, Technion - Israel Institute of Technology, Haifa, 32000 Israel (e-mail: oriane, dudi74@tx.technion.ac.il, zeevi@ee.technion.ac.il).

Under some mild assumptions, it is possible to separate the mixtures back into the sources. This is done either by estimating the mixing matrix $\hat{A}$ [2] and calculating the matrix $\hat{W} = \hat{A}^{-1}$, or by estimating directly $\hat{W}$ [3]. Both methods yield the estimated vector $\hat{S}$ of the original sources:

$$\hat{S} = \hat{W} \cdot X. \tag{2}$$

For reasons inherent in the problem formulation, $\hat{A}$ is an estimation of A up to column permutation and scaling.

We solve the BSS problem by means of geometrical Sparse Component Analysis (SCA) [2]. This approach is based on the assumption that the sources can be sparsely represented by using a linear transform Φ (neglecting n):

$$\Phi[X(\gamma)] = A \cdot \Phi[S(\gamma)]. \tag{3}$$

In this study we achieve such a sparsification in two ways: (i) multiscale wavelet packets (ii) multiscale Curvelet transform. We then exploit the properties of the sparse representation, obtained by projection of the mixtures onto the sparse space and constructing the scatter plot of one sparsely-represented mixture versus the other. This approach, presented in detail in [2], assumes that in the space of sparse representation, most of the data points are contributed primarily by only one source. Consequently, they are co-linearly clustered along m lines, corresponding to the columns of the mixing matrix [2]. For example: considering equation (3), we assume $\Phi[S(\gamma)]$ to be a sparse vector. Sparsity claims that for every γ, all elements of $\Phi[S(\gamma)]$ vanish except one. The columns of the sparsified vector $\Phi[X(\gamma)]$ therefore yield:

$$\begin{aligned} \Phi[x_{1\gamma}] &= a_{1k} \cdot \Phi[s_{k\gamma}] \\ \Phi[x_{2\gamma}] &= a_{2k} \cdot \Phi[s_{k\gamma}], \end{aligned} \tag{4}$$

assuming $S_{k\gamma}$ to be a dominant coefficient, and $A_{2\times m}$. Thus, we have $[a_{1k}\ a_{2k}]^T$ as a column of A, up to scaling. The process of equation 4 can of course be repeated for every number of mixtures and sources.

II. METHODS

A. Image Data

Two sets of data have been employed in the assessment of the proposed technique: (i) Simulated Data: obtained from BrainWeb MRI Simulator, available at [4]. (ii) Clinical MR images: Obtained using a 1.5T GE-Healthcare machine, scanning a 26 year old healthy male.

B. Pre-Processing:

In order to get optimal results, a block-shaped ROI inside the brain image was selected. Our model of fat and water as creating sources does not include the bone, muscle and connective tissue in the skull. Therefore, the skull region of the image was 'cut out'. This was done either manually, or through automated morphological analysis.

C. Processing:

All processing was done using a Matlab code running on standard PCs. Wavelets analysis functions are available in the Matlab Wavelet Processing toolbox. Curvelet analysis functions are available at [5]. Ultimately, for the separation model described in this work, two images (mixtures) should suffice for recovery of 2 sources. However, in order to overcome noise and similar problems, we process a set of 3 images (mixtures) at a time.

D. Post-Processing:

(i) Node selection: Using multiscale analysis, a large set of nodes is created. The problem of node selection is discussed in [2] and [6], without final conclusion. In this work, the nodes were reviewed and selected manually.

(ii) Having obtained the multi-scale analysis coefficients, we classify them into clusters. The orientation of these clusters make the columns of the estimated mixing matrix $\hat{A}$ [2]. The Data distribution is ruled by the existence of the sparse representation hypothesis, i.e. that most of the data points in the sparse space are contributed by only one source. When the hypothesis condition is not perfectly fulfilled, and the mixtures are subject to additive noise, outliers become dominant in the estimation of the data orientations. thus the outliers must be considered in the estimation of the orientations, This is done either through Iterative Fuzzy K-means (FCM), based on [7], or Iterative Robust Multiple Regression, based on [8]. Using Iterative-FCM, only points with high membership weights towards their orientation-centroid were kept for additional iteration. The process is repeated until convergence of the orientations is achieved, or until some termination criteria is met. Using robust regression, different weighting functions are used to detect and give less significance to outliers in the regression calculation. Weighting is generally given according to some outlier criteria; data points are sorted according to it, and given their weight according to their index in the sorted data vector. The sorting criterion that was used is the mean square distance of each data point to the previous estimated orientation. Since the existence and influence of outliers is ruled by the dimension of the problem, an exponential weighting function was chosen with its exponent proportional to the number of mixtures. The data points with the highest norm were trimmed. The resulted weighting function is:

$$W_i = \begin{cases} (i/\hat{\sigma}_c)^{-f(dim)} & i \le i_{th} \\ 0 & i > i_{th} \end{cases}$$

where i is the index of the sorted data point and i_{th} is a threshold index. $\hat{\sigma}_c$ is an estimate of the data points variance about their orientation. $f(dim)$ is a real positive function, and dim is the number of given mixtures, which is the dimension of the space of sparse represantation. Since the different data populations coexist in the sparse space, implementation of the robust regression is performed by two stages: First, each data point is clustered to its nearest orientation. Then, regression is applied to each cluster separately, and a new orientation is calculated.

(iii) Since the estimated mixing matrix columns are given up to scaling and polarity, we have to estimate what is the 'correct' direction (For 2 sources, 4 polarity combinations exist). While a comparison of the results versus a training set produced the best results, Joint Entropy, Mutual Information [9] and Sources Covariance were examined as well.

Generally, apart from the manual transform-node selection, the entire processing time is about 20 seconds, using a 1.8 GHz Intel Centrino.

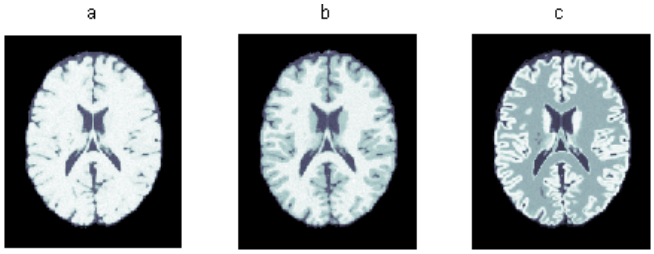

Fig. 1. Simulated spoiled FLASH images: (a) Tr=75 Te=75, (b) Tr=125 Te=10, (c) Tr=250 Te=250. Time is given in [msec].

III. Results

We demonstrate our approach on both simulated MR data [4], and clinically acquired MR images. The simulated data is used in order to compare the performance of the proposed method with available ground-truth.

A. Simulated Images:

Three 1 mm thick slices were acquired using the spoiled FLASH scan technique with *Tr=[75, 125, 250] msec* and *Te=[75, 10, 250] msec*. This results in having different weights of the inhabiting substances (Fig. 1). 'White' noise in magnitude of 3% of the brightest tissue is added. Two-dimensional wavelet packet analysis, using the 1st and 2nd order Daubechies Wavelets, is performed. Following analysis, coefficient from the (1,2) node of the transform are selected. The decomposition coefficients are then projected onto the observations space to form a scatter-plot (Fig. 2).

Each co-linearly clustered partial set of data of the scatter-plot indicates the existence of a source. The underlying linear mixing model is confirmed by this unique clustering configuration. The dominant orientations are estimated using a suitable optimization algorithm: FCM or Robust Regression. This yields the estimate entries of the linear mixing matrix. Fig. 3 illustrates the result of the sparisification operation, when the skull is not removed. One or more additional sources are found. The existence of such source is indicated

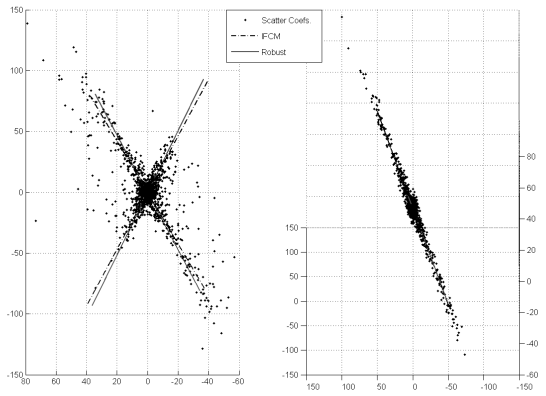

Fig. 2. Scatter plot of the sparsely represented mixtures using wavelets on simulated data. Two dominant orientations are visible. Left: 'Top View'. Right:'Side View', revealing a plane.

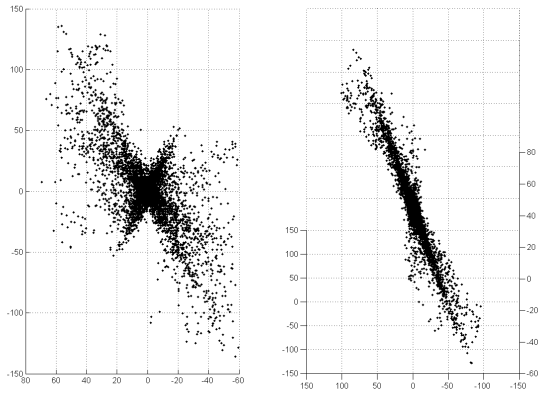

Fig. 3. Scatter plot of the simulated data, without removing the skull. Several dominant orientations emerge. Left: 'Top View'. Right: 'Side View', revealing co-linear clusters out of the expected plane.

by an 'out of plane' cluster, compared with the clusters in the trimmed image (Fig. 2).

Using pseudo inverse, the corresponding sources are then recovered. These turn out to be the water and fat source images. The bright regions of the fat image (Fig. 4a) correspond to the white matter tissue, and the bright regions of the Water image (Fig. 4b) correspond to the cerebrospinal fluid (CSF). Fig. 4a-d depict a comparison of the recovered sources and the available ground-truth tissues.

These recovered sources enable further classification to CSF, grey matter and white matter (Fig. 4e), by mapping pixels combinations of sources according to a look-up table, reflecting the known characteristic composition of brain tissue.

B. Clinical Images:

A set of clinical MR images (spin-echo technique, *Tr=[500, 500, 2400] msec* and *Te=[8, 20, 20] msec*) was acquired (Fig. 5) and analyzed.

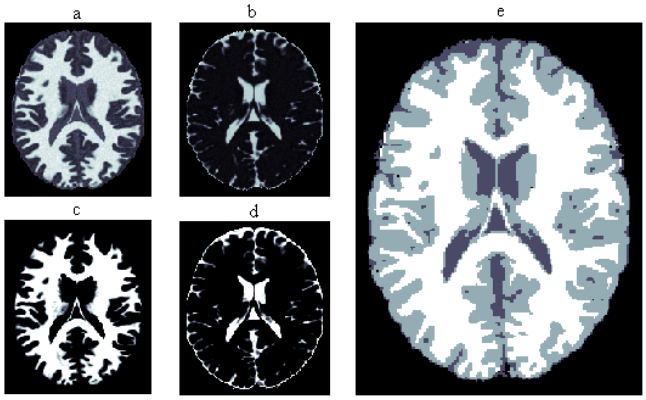

Fig. 4. images a-d: Top Row: Recovered sources. Bottom row: Original tissues. Left column: Bright regions correspond to White matter. Right column: Bright regions correspond to CSF.
image e: Classification of the **recovered** brain tissue-White matter (White), Grey matter (Grey), CSF (Dark Grey).

1) Wavelet Analysis: Node (1,2) of a 2D wavelet transform was selected again. This time, we combined the coefficients of several wavelet transforms: 'sym2', 'sym3', 'coif1', 'bior2.2', 'bior4.4' and 'bior6.8'. Only a fraction of the coefficients were used, 0.5% coefficients with highest L2 norm. The scatter plot is given in Fig. 6a. We use FCM to estimate the dominant orientations, corresponding to the columns of $\hat{A}$. Following that, the sources Fat and Water were extracted (Fig. 7a and 7b). Using a look-up table we classify to White, Grey matter and CSF, see Fig. 7c.

2) Curvelet Analysis: A second estimation of the mixing matrix was performed, using Fast Discrete Curvelet Transform (FDCT) [5]. The sparse Nodes of the transformed data tree, depicting best sparsification, were manually selected. Only 0.5% of the highest L2 norm coefficients were used to produce the scatter plot in Fig. 6b. The dominant orientations were normalized to unit vectors and compared with the vectors obtained through wavelet analysis (Fig. 6 and Table 1): The estimated orientations and the illustration in fig. 6a-b display consistent orientations, and accepetable error, due to inherent noise in the images. Since the FDCT transforms from $\mathbb{R}^{n\times n}$ to $\mathbb{C}^{n\times n}$, every selected node actually provides 2 sets of coefficients: one real and one imaginary, Both are projection to sparse spaces, as validated over synthetic images and mixtures prior to application to MR data.

$$\hat{A}^{FCM}_{Wave}=\begin{pmatrix} -0.588 & 0.556 \\ -0.395 & 0.528 \\ 0.706 & 0.642 \end{pmatrix} \hat{A}^{FCM}_{FDCT}=\begin{pmatrix} -0.574 & 0.561 \\ -0.424 & 0.531 \\ 0.701 & 0.636 \end{pmatrix}$$

$$\hat{A}^{Robust}_{Wave}=\begin{pmatrix} -0.571 & 0.557 \\ -0.305 & 0.554 \\ 0.762 & 0.619 \end{pmatrix} \hat{A}^{Robust}_{FDCT}=\begin{pmatrix} -0.512 & 0.524 \\ -0.385 & 0.568 \\ 0.768 & 0.635 \end{pmatrix}$$

Table 1: Estimation of the mixing matrix using different combinations of multiscale transforms and orientation estimation methods. FCM-Fuzzy K-means, Robust-Robust Regression, Wave-Wavelet Trans., FDCT-Curvelet Trans.

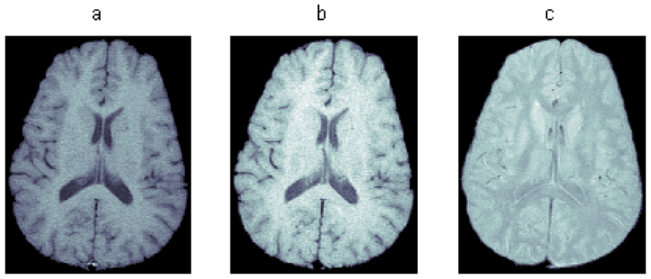

Fig. 5. Clinical Spin-Echo MR images - From left to right: (a) Tr=500, Te=8 (b) Tr=500, Te=20 (c) Tr=2400, Te=20 All times in [msec].

IV. Discussion

(i) The results presented in this paper demonstrate that sparse representation of MR images is possible, using off-the-shelf sparsification techniques. Since the simulated and clinical data have somewhat different geometrical and anatomical features, a dictionary comprised of more than one type of wavelet had to be used. The low SNR clinical data results in less than optimal sparseness and co-linearity of the projected images. This suggests that one should search for special types of wavelets, optimally designed to fit the properties of the MR images.

(ii) Using combined multi-scale transforms, a large set of nodes is created, giving rise to problem of selecting significant and sparse nodes ? Some critical facets of this problem include: **a)** While 2 or more sources may exist, some nodes display sparse coefficients for only one of the sources. The curvelet transform of the simulated data produced only one strong orientation, in almost all of its nodes. **b)** A large set of coefficients corrupted with crosstalk errors are concentrated in relative low magnitudes. A low magnitude in one node may be considered a high magnitude in another. Therefore, adaptive thresholds are required to deal with the problem.

(iii) Noise and magnetic field non-uniformity are inherent in the MR technology. While the human eye is less sensitive to the resultant distortions, the resultant sparsity (Fig. 6) and tissue classification (Fig. 7) are affected to a greater extent, compared with the simulated data. Employing a block-coordinate approach improves the results.

(iv) Practical use: Figures 2 and 6 validate the model of the brain tissue image as a mixture of two sources, fat and water. Figure 3 illustrate that when external tissues (attributed to skull bones, muscles and connective tissue) are added, additional co-linear cluster appear. If the number of expected sources and clusters is known, additional clusters indicate the existence of a foreign tissue or object. Since many multi-scale transforms are localized in space, the pixels creating the unexpected clusters can be traced. This can be an alert and segmentation aid for the clinical personal.

The figures presented in this paper are available at: http://visl.technion.ac.il/bss/embc2006.

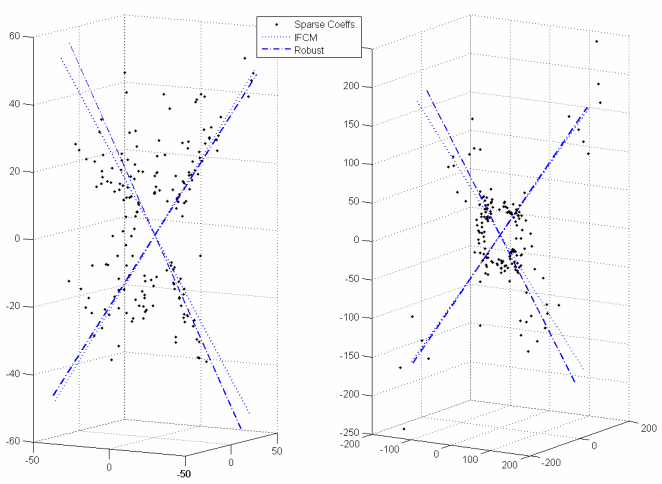

Fig. 6. Clinical images multi-scale analysis - Left to right: (a) Selected coefficients of the wavelet transform. (b) Selected coefficients of the curvelet transform. In both scatter plots, two dominant orientation emerge.

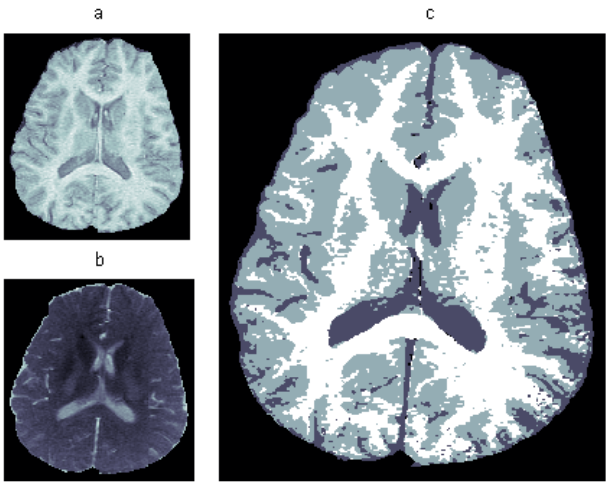

Fig. 7. Estimated sources: (a) Bright regions correspond to Fat source. (b) Bright regions correspond to Water source. (c) Recovered brain tissue classification: white matter (white). grey matter (grey). CSF (dark grey).

References

[1] W. Thomas Dixon, *Simple Proton Spectroscopic Imaging*, Radiology, Vol. 153, pp. 189- 194,1984.

[2] P. Kisilev, M. Zibulevsky and Y.Y. Zeevi, *A Multiscale Framework For Blind Source Separation*, Journal of Machine Learning Research Vol. 4, pp. 1339-1363,2003.

[3] A.M. Bronstein, M.M. Bronstein, M. Zibulevsky, *Blind source separation using block-coordinate relative Newton method*, Signal Processing 84 (2004) 1447 - 1459.

[4] BrainWeb 3D MRI simulated brain database - http://www.bic.mni.mcgill.ca/brainweb

[5] E. J. Candes, L. Demanet, D. L. Donoho, L. Ying, *Fast Discrete Curvelet Transforms*, 2005, available at www.curvelet.org..

[6] A. M. Bronstein, M. M. Bronstein, M. Zibulevsky, Y. Y. Zeevi, *Sparse ICA for blind separation of transmitted and reflected images*, Intl. Journal of Imaging Science and Technology (IJIST), Vol. 15/1, pp. 84-91, 2005.

[7] J. C. Bezdek (1981): *Pattern Recognition with Fuzzy Objective Function Algoritms*, Plenum Press, New York

[8] Rousseeuw, P.J. and Leroy, A.M. (1987), *Robust Regression and outlier detection* , Wiley-Interscience, New York (Series in Applied Probability and Statistics).

[9] T.M. Cover, J.A. Thomas, *Elements of Information Theory*, Wiley Series in Telecommunications (2001), Hoboken, N.J. Available online at: http://www3.interscience.wiley.com/cgi-bin/bookhome/86512731